Journal of Electronic Materials
https://doi.org/10.1007/s11664-024-11387-0

28TH INTERNATIONAL CONFERENCE ON NUCLEAR TRACKS AND RADIATION MEASUREMENTS

Green Synthesis of Copper Sulphide Nanoparticles Using Extracts of *Syzygium cumini*, *Azadirachta indica*, and *Cascabela thevetia*

KM Srishti Barnwal[1] · Yukti Gupta[1] · Neena Jaggi[1]

Received: 27 December 2023 / Accepted: 14 August 2024

Abstract
Nanotechnology is a burgeoning modern technology due to the remarkable properties of nanoparticles. However, the escalating use of toxic reagents during the chemical synthesis of nanoparticles has become a major concern for environmental safety and human and animal health. Regarding this problem, the notion of integrating nanotechnology with green synthesis is increasingly attracting the attention of researchers. This particular study aims at the green synthesis of copper sulphide (CuS) nanoparticles S1, S2, and S3 utilizing the leaf extracts of *Azadirachta indica* (neem), *Syzygium cumini* (jamun), and *Cascabela thevetia* (kaner), respectively. The prepared leaf extract of neem is rich in quercetin, whereas extracts of jamun and kaner leaves contain gallic acid, which serves as a reducing agent during the formation of nanoparticles. The prominent and sharp peaks of x-ray diffraction (XRD) patterns match well with ICDD card no. 06-0464, which confirms the hexagonal phase of covellite CuS. Scanning electron microscopy (SEM) images reveal the formation of spherical-shaped CuS nanoparticles with mild agglomeration. The presence of Cu and S as the only elements in the synthesized samples is confirmed by energy-dispersive x-ray analysis (EDX). The occurrence of various stretching and bending vibrational modes is observed via Fourier transform infrared (FTIR) spectroscopy. Furthermore, the obtained FTIR spectra of S1, S2, and S3 evince the formation of CuS nanoparticles and the presence of bioactive compounds. The UV-Vis absorption data of the prepared samples reveal that their band gap energies lie within the range of 1.5–1.7 eV. The photoluminescence (PL) spectra of S1, S2, and S3 display decreased intensity, which could be due to the reduced recombination rate of charge carriers. The CuS nanoparticles synthesized with neem leaf extract exhibit relatively smaller crystallite size, wider band gap of 1.7 eV, and a lower recombination rate of charge carriers.

Keywords Nanotechnology · green synthesis · bioactive compounds · CuS nanoparticles

Introduction

Nanoparticles of the transition metal chalcogenides group have garnered enormous attention from researchers in recent years because of their astounding catalytic, optical, and optoelectronic properties.[1,2] Copper sulphide (Cu_xS, where $x = 1–2$) is a relatively non-toxic chalcogenide. It occurs in several crystalline phases with different stoichiometric compositions such as covellite (CuS), anilite ($Cu_{1.75}S$), digenite ($Cu_{1.8}S$), djurlite ($Cu_{1.95}S$), and chalcocite (CuS_2). It also exhibits various lattice structures from orthogonal to hexagonal.[1,3–5] The optical, electrochemical, and electrical properties of CuS nanoparticles are governed by their stoichiometry, size, morphology, and crystal structure.[6] Bulk CuS shows a forbidden energy gap ranging between 1.2 eV and 2.89 eV.[1] It is a *p*-type metal chalcogenide semiconductor with a direct optical band gap, since Cu vacancies in it serve as electron acceptors. At nanoscale, the energy band gap of nanoparticles increases due to the effect of quantum confinement.[7] CuS nanoparticles show a wide range of absorbance in the ultraviolet (UV), visible, and near-infrared (NIR) regions depending on their broad optical band gap energy.[8,9] The energy band gap can be tuned by modifying the size and morphology of nanoparticles.[6,8,10–13] The published research data reveal that synthesizing CuS nanoparticles is an intricate process, as Cu and S both exist in two different

✉ KM Srishti Barnwal
srishti215barnwal@gmail.com

[1] Department of Physics, National Institute of Technology Kurukshetra, Thanesar, Haryana 136119, India

Published online: 03 September 2024

oxidation states, Cu^{+1}, Cu^{+2}, $(S)_2^{-2}$, and S^{-2}, respectively, and thus the growth of nanoparticles is difficult to control.[8] To overcome this issue, several preparatory methods have been proposed for the chemical synthesis of CuS nanoparticles, including sol–gel, chemical co-precipitation, hydrothermal, solvothermal, microwave, hot injection, and sonochemical techniques. However, the need for toxic chemical-based reducing agents, stabilizing agents, and solvents limits the use of these techniques.[14–19]

There are potential benefits of synthesizing nanoparticles via green synthesis rather than chemical routes. Green synthesis can be considered as a non-hazardous, sustainable, economical, easily controlled, scalable, biocompatible, and flexible alternative that promotes the synthesis of biocompatible nanoparticles.[20] Plant extracts with medicinal properties contain several bioactive constituents including flavonoids, terpenoids, polyphenols, ascorbic acid, alkaloids, phenolic acids, sugar, and protein which reduce the size of nanoparticles.[21–23]

Over the past few years, several approaches for synthesizing metal chalcogenide nanoparticles via the green route have been reported by researchers. Slathia et al. synthesized Ag-ZnO nanocomposite using leaf extracts of *Azadirachta indica* via a facile hydrothermal approach. The extract was prepared using two different solutions such as double-distilled water and ethanol. They also studied the electrical and optical properties of the synthesized Ag-CuS samples. The green-synthesized Ag-CuS nanocomposite shows potential for effective use in fluorescence-based sensors.[24] Ullah et al.[25] examined the photocatalytic properties of cadmium sulfide (CdS) nanoparticles synthesized using plant extracts of *Dicliptera roxburghiana* via a green route for the degradation of hazardous organic dyes. Rawat et al.[26] studied the effect of heating on green-derived CuS nanoparticles by synthesizing CuS nanoparticles via leaf extracts of *Urtica dioica* and found that the crystallinity of samples increases with heat treatment. Bonigala et al.[27] reported the green synthesis of Au nanoparticles using extracts of *Cascabela thevetia* (leaves), *Stemona tuberosa* (whole plant), *Wrightia tomentosa* (leaves), and *Rauvolfia serpentina* (roots) in separate reactions. Riaz et al. provided a detailed research study on the synthesis of NiO nanoparticles using leaf extract of *Syzygium cumini*. They calculated a crystallite size for NiO nanoparticles of 10.4 nm. Antioxidant activity of CuS samples was analysed using 2,2-diphenyl-1-picrylhydrazyl (DPPH) free radical scavenging activity.[28] Savarimuthu et al.[9] explored the fast degradation of dyes with or without sulphite under dark conditions via CuS nanoparticles by green synthesis using rice starch water. Gupta et al.[20] synthesized covellite CuS nanoparticles via an integrated hydrothermal-green synthesis route using an aqueous extract of *Ocimum tenuiflorum* (tulsi) and studied its enhanced optical properties.

Apart from these plant-based extracts, some plants are still unexplored for the synthesis of CuS nanoparticles. Neem is a well-known medicinal tree with antiseptic, anti-inflammatory, anti-allergic, immunomodulatory, antioxidant, antimalarial, and anti-carcinogenic properties.[29] The major constituent of the neem leaf extract is quercetin, a bioactive flavonoid compound that reduces metal ions to nanoparticles.[30] The extract of jamun leaves contains gallic acid as the main reducing agent, while jamun leaves have anti-diabetic, anti-inflammatory, antioxidant, diuretic, digestive, and carminative properties.[31] In addition, kaner leaf extract is rich in polyphenolic compounds or phenolic compounds with many hydroxyl groups including ellagic and gallic acid as prominent reducing agents. The presence of cardenolides in the extract highlights its potential application in the treatment of cardiac failure.[32]

A facile hydrothermal approach for synthesizing CuS nanoparticles using leaf extracts of *Azadirachta indica* (neem), *Syzygium cumini* (jamun), and *Cascabela thevetia* (kaner) is explored for the first time to the best of our knowledge. The leaf extracts of neem, jamun, and kaner plants were utilized as solvents to synthesize CuS nanoparticles. The structural and phase analysis, morphological study, elemental identification, analysis of functional groups, and optical characterization of the green-synthesized samples were conducted via x-ray diffraction (XRD), scanning electron microscopy (SEM), energy-dispersive x-ray spectroscopy (EDX), Fourier transform infrared (FTIR) spectroscopy, ultraviolet–visible (UV-Vis) spectroscopy, and photoluminescence (PL) spectroscopy. A reduction in the average crystallite size and decreased particle size of the synthesized CuS nanoparticles were observed. The neem-based CuS sample exhibited relatively higher absorbance in the visible region, with an energy band gap of 1.7 eV, which occurs due to quantum confinement at the nanoscale.

Experimental

Chemicals and Materials

In this investigation, copper nitrate trihydrate [$Cu(NO_3)_2.3H_2O$, ~ 95–103% purity (CAS no-C15029)] and sodium sulphide [Na_2S, ~ 60% purity (CAS no-27610-45-3)] were used as Cu and S precursors, respectively, to synthesize covellite CuS nanoparticles. The high-quality and high-purity chemicals were procured from Nice Chemicals and Loba Chemie, respectively. Deionized (DI) water was used for preparing the leaf extracts and washing purposes. Ethanol was also used for the final washing of autoclaved samples. Leaves of neem (*Azadirachta indica*), kaner (*Cascabela thevetia*), and jamun (*Syzygium cumini*) were collected from

the campus square of the National Institute of Technology, Kurukshetra, Haryana, India.

Green Synthesis

Preparation of Leaf Extracts

The freshly collected leaves were cleaned by washing them several times with DI water to clear away the dirt particulates and other impurities. The washed leaves were chopped into small pieces and placed in a hot air oven for drying at 80°C for 6 h. Afterward, the dried leaves were pulverized into fine powder using an electrical grinder. Next, 3 g of finely powdered neem leaves was heated in 120 mL DI water in a beaker with continuous stirring for 2 h using a magnetic stirrer at a constant temperature of 60°C. After cooling to room temperature, the leaf extract was filtered out using a Buchner funnel equipped with Whatman no. 1 filter paper. The same procedure was used to prepare kaner and jamun leaf extracts.

Plant Metabolite-Based CuS Synthesis

For the green synthesis of copper sulphide nanoparticles, the hydrothermal route was followed as displayed in Fig. 1. Initially, $Cu(NO_3)_2.3H_2O$ (0.5 M) was added to 30 mL neem leaf extract and was continuously stirred mechanically using a magnetic stirrer for 1 h. A similar process was followed simultaneously for preparing Na_2S (1 M) in 30 mL neem leaf extract which was added in drops to the previously prepared solution. Afterward, the mixture was stirred for 30 min to get a well-homogenized solution. Then the mixture was transferred to an autoclave which was positioned in a hot air oven at 125°C for 12 h to allow the chemical reactions to occur. The black precipitate was separated from the solution using double-filtration via Whatman filter no.1 and washed using DI water and ethanol to eliminate soluble contaminants. The filtered precipitate was dried in the oven. The dried sample was ground into a uniform powder using a mortar and pestle. Following an identical process, CuS nanoparticles were also prepared using kaner and jamun extracts.

Characterization

The diffraction planes and the crystallite phase identification of the synthesized CuS samples were determined by XRD patterns, using a Bruker AXS D8 Advance diffractometer with Ni filtered Cu-Kα radiation ($\lambda = 0.154$ nm) within 2θ range of 25°–70° functioning at a scanning speed of 0.05°/min. The green-synthesized samples were examined for surface morphology analysis by scanning electron microscopy (SEM) using a JEOL JSM-6390 JV instrument. EDX spectra were recorded to ascertain the elemental identification. UV–Vis spectroscopy was used to study the optical band gap energies of all samples via a Shimadzu UV-2600i UV–Vis spectrophotometer. PL analysis of CuS samples was conducted using a Shimadzu RF-5301PC

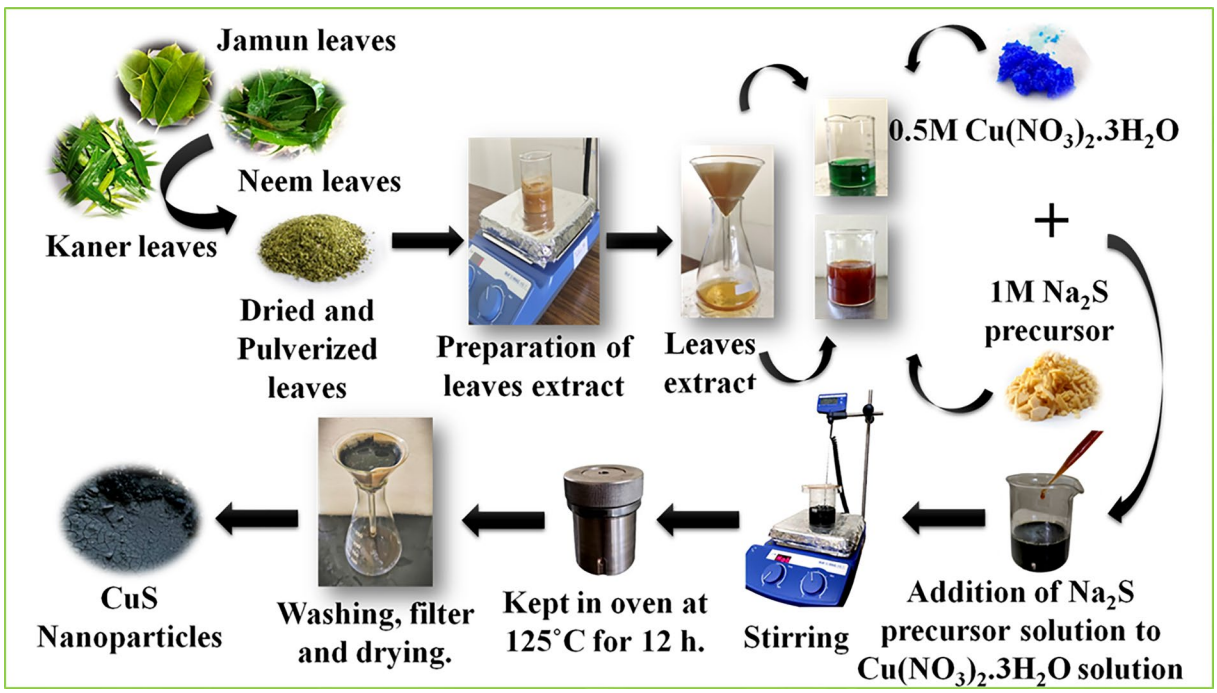

Fig. 1 Synthesis route for synthesizing CuS nanoparticles using leaf extracts of neem, jamun, and kaner.

spectrofluorophotometer to study the electronic transitions of photoinduced electrons between the highest occupied molecular orbital (HOMO) of the valence band and lowest unoccupied molecular orbital (LUMO) of the conduction band of CuS nanoparticles The functional groups present in the CuS samples were analysed by FTIR spectra recorded via an MBB-3000 ABB FTIR spectrophotometer.

Results and Discussion

Green Synthesis Growth Mechanism for CuS Nanoparticles

The leaf extracts were prepared by heating the powdered leaves in DI water with continuous magnetic stirring as represented in Eq. 1. DI water is an effective polar solvent which exhibits good affinity for polar compounds such as phenolic acids, esters, and glycosides present in the leaf extracts. The polar compounds exhibit good solubility in aqueous solvent and can be easily extracted using DI water under certain conditions.[33] The temperature was maintained constant at 60°C for 2 h during the extraction of leaf extracts. At this temperature and within this time duration, phenolic compounds remain stable in the extraction solvent.[34]

$$\text{Pulverized leaves} + \text{DI} \xrightarrow{\Delta} \text{Leaf extract} \quad (1)$$

The major reducing bioactive compound present in the leaf extract of neem is quercetin ($C_{15}H_{10}O_7$).[35] Quercetin is a flavonoid with a three-ring structure having five hydroxyl groups. Interaction of quercetin with Cu^{2+} and S^{2-} leads to the formation of CuS nanoparticles.[24] The leaf extracts of jamun and kaner are rich in gallic acid ($C_7H_6O_5$),[27,36] which is a phenolic compound with a single aromatic ring consisting of three hydroxyl groups, which promotes reduction of metal ions to metal nanoparticles.[22,37,38] The reaction occurring during the synthesis process can be determined from Eq. 2. Variations in colour of the final samples are detected, ranging from dark brownish black to dark bluish black which evidences the formation of CuS nanoparticles.

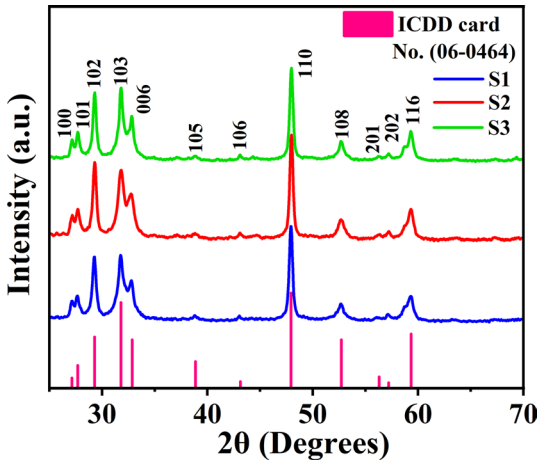

Fig. 2 The diffraction peaks of CuS samples using XRD patterns.

$$Cu(NO_3)_2.\,3H_2O + Na_2S \xrightarrow[C_7H_6O_5]{C_{15}H_{10}O_7} CuS + 2\,NaNO_3 \quad (2)$$

Structural Analysis

The x-ray diffraction (XRD) pattern was recorded to evaluate the crystallite size and the phase purity of all prepared samples as shown in Fig. 2. The recorded data match well with ICDD card no. 06-0464 confirming the hexagonal covellite phase of CuS. The obtained diffraction peaks for green-synthesized samples corresponding to (100), (101), (102), (103), (006), (105), (106), (110), (108), (201), (202), and (116) Miller planes of CuS assured the polycrystalline nature of all three samples. The prominent sharp and strong diffraction peaks for S1 are positioned at 2θ values 27.14, 27.70, 29.31, 31.83, 32.79, 38.88, 43.11, 48.00, 52.68, 56.26, 57.26, and 59.38 indexing to (100) (101), (102), (103), (006), (105), (106), (110), (108), (201), (202), and (116) planes of CuS, respectively. The obtained XRD profile of S2 indicates a slight right shift of 0.05 corresponding to S1. The XRD pattern of S1 depicts a slight widening of peaks which leads to an increase in the full width at half maximum (FWHM) of peaks. S1 displays comparatively reduced crystallite sizes of CuS nanoparticles as the FWHM of the XRD peaks and crystallite size are inversely correlated as shown in Table I. The decrease in crystallite size results in decreased crystal alignment and thus a broadening of the XRD peaks.[39] The standard values for lattice parameters of the hexagonal phase of covellite CuS nanoparticles are $a = b = 0.379$ nm and $c = 1.634$ nm. The calculated values of lattice parameters as mentioned in Table II are approximately close to the standard values of lattice parameters of covellite CuS.

The interplanar spacing (d_{hkl}) and crystal lattice parameters *a, b,* and *c* for S1, S2, and S3 are evaluated by using Bragg's law in Eqs. 3 and 4.[40]

Table I Parameters of the XRD, the peak position values (2θ), *d*-spacing, FWHM, Miller indices, and the corresponding crystallite size for the preferred peaks of as-synthesized samples S1, S2, and S3

Sample name	2θ, degrees	FWHM, degrees	*d*-spacing, nm	Planes	Crystallite size, nm
S1	27.634	1.054	0.322	(101)	7.752
	29.322	0.529	0.304	(102)	15.506
	31.816	0.887	0.281	(103)	9.308
	32.788	0.854	0.273	(006)	9.691
	47.986	0.471	0.189	(110)	18.450
	59.160	1.074	0.157	(116)	8.495
S2	27.688	1.096	0.322	(101)	7.460
	29.380	0.426	0.303	(102)	19.250
	31.900	0.743	0.280	(103)	11.113
	32.858	0.691	0.272	(006)	11.989
	48.051	0.411	0.189	(110)	21.110
	59.291	0.970	0.155	(116)	9.420
S3	27.560	0.944	0.323	(101)	8.662
	29.278	0.411	0.304	(102)	19.952
	31.789	0.692	0.281	(103)	11.939
	32.749	0.683	0.271	(006)	12.112
	47.954	0.407	0.189	(110)	21.314
	59.202	1.018	0.155	(116)	8.969

Table II Lattice strain and dislocation density computed from XRD data for all CuS samples

Sample name	Lattice parameters (nm)		Dislocation density ($\times 10^{15}$), nm	Lattice strain ($\times 10^{-3}$)
	(a = b)	c		
S1	0.378	1.638	9.963	11.112
S2	0.378	1.632	8.205	9.923
S3	0.378	1.626	7.384	9.372

$$d_{hkl} = \frac{n\lambda}{2\sin\theta} \tag{3}$$

$$\frac{1}{d^{2hkl}} = \frac{4}{3}\frac{h^2 + hk + k^2}{a^2} + \frac{l^2}{c^2} \tag{4}$$

where n represents the order of diffraction, θ is the angle of diffraction, λ is the x-ray wavelength with a value of 0.154 nm, d represents the spacing between diffracting planes, (hkl) is the Miller planes, and the lattice constants between the adjacent unit cells of a crystal lattice are a, b, and c.

The crystallite size corresponding to each Miller plane is calculated using the Debye-Scherrer formula, i.e. Eq. 5.[39]

$$D = \frac{k\lambda}{\beta * \cos\theta} \tag{5}$$

where D denotes average crystallite size, k indicates the shape factor (0.94 for spherical particles), the x-ray wavelength is λ, β is the FWHM (the full width at half maximum of x-ray diffraction peaks), and θ is Bragg's angle of diffraction.

The lattice strain (ε) arises because of the crystal imperfections such as varying crystallite size and lattice dislocation, which is calculated by applying Eq. 6.[20]

$$\varepsilon = \frac{\beta}{4\tan\theta} \tag{6}$$

where ε is lattice strain and β is the FWHM of XRD peaks. The dislocation density (δ) defines the number of dislocations per unit volume of the crystal lattice which is determined by applying Eq. 7.[41]

$$\delta = \frac{1}{D^2}\ \mathrm{nm}^{-2} \tag{7}$$

All calculated values such as interplanar spacing, crystallite size, lattice parameters, dislocation density, and lattice strain of the synthesized samples are presented in Tables I and II.[21]

Table I shows that different leaf extracts used in the synthesis of CuS nanoparticles affect the crystallite sizes of nanoparticles. In Table II, the monotonic decrease in the computed values of lattice strain for S1, S2, and S3 is due to an inverse relation between crystallite size and the

strain produced in the lattice.[42] The dislocation density also decreases with an increase in the crystallite size of nanoparticles. Sample S1 exhibits the smallest crystallite size of 18.45 nm corresponding to the (110) plane. This may cause an increase in the energy band gap of sample S1, which reduces the rate of recombination of charge carriers and enhances its optical properties.[43]

Morphological Properties

SEM was used to analyse the surface morphology of the green-synthesized CuS samples. Figure 3a–c displays the SEM images of CuS nanoparticles synthesized using leaf extracts of neem, jamun, and kaner, respectively, at a magnification of ×10,000 and a scale of 1 µm. SEM images show the formation of spherical-shaped CuS nanoparticles with slight agglomeration. The SEM image of S1 depicted in Fig. 3a confirm the synthesis of spherical-shaped nanoparticles with minimal agglomeration. Figure 3b exhibits the SEM image of S2, which shows the spherical morphology of the sample with slightly agglomerated nanoparticles. SEM analysis of S3 shows the synthesis of spherical-shaped nanoparticles with mild agglomeration as shown in Fig. 3c. S3 displays a relatively better morphology, which may be attributed to its relatively small dislocation density and lattice strain values. SEM analysis of the synthesized samples shows a noticeable non-uniformity in the size of nanoparticles, which could be due to the presence of bioactive compounds in the sample.

The particle size of CuS nanoparticles was determined by histogram analysis obtained from SEM data using ImageJ software as illustrated in Fig. 3d–f. Figure 3d presents the histogram data for S1 which shows an average particle size of 112.57 nm for neem-mediated CuS nanoparticles. Figure 3e shows an average particle size of 168.94 nm for S2, while an average particle size of 184.22 nm for the S3 sample is shown in Fig. 3f.[32] The smallest average particle size is obtained for the synthesized sample with neem leaf extract and leads to the increased energy band gap of CuS nanoparticles.[44]

Energy-Dispersive X-ray (EDX) Analysis

The elemental configuration and % of all elements present in the synthesized CuS samples were analysed and determined using EDX spectra. The obtained EDX data represent the formation of CuS nanoparticles by confirming the presence of Cu and S as major elements, as shown in Fig. 4a–c. The % atomic compositions of Cu and S in all samples are presented in Table III. The elemental analysis of Cu and S in terms of at.% present in samples synthesized using different leaf extracts displays almost the same stoichiometric ratio of 1:1, which confirms the formation of CuS nanoparticles.[20] The EDX data of S1 are comparatively more similar to the

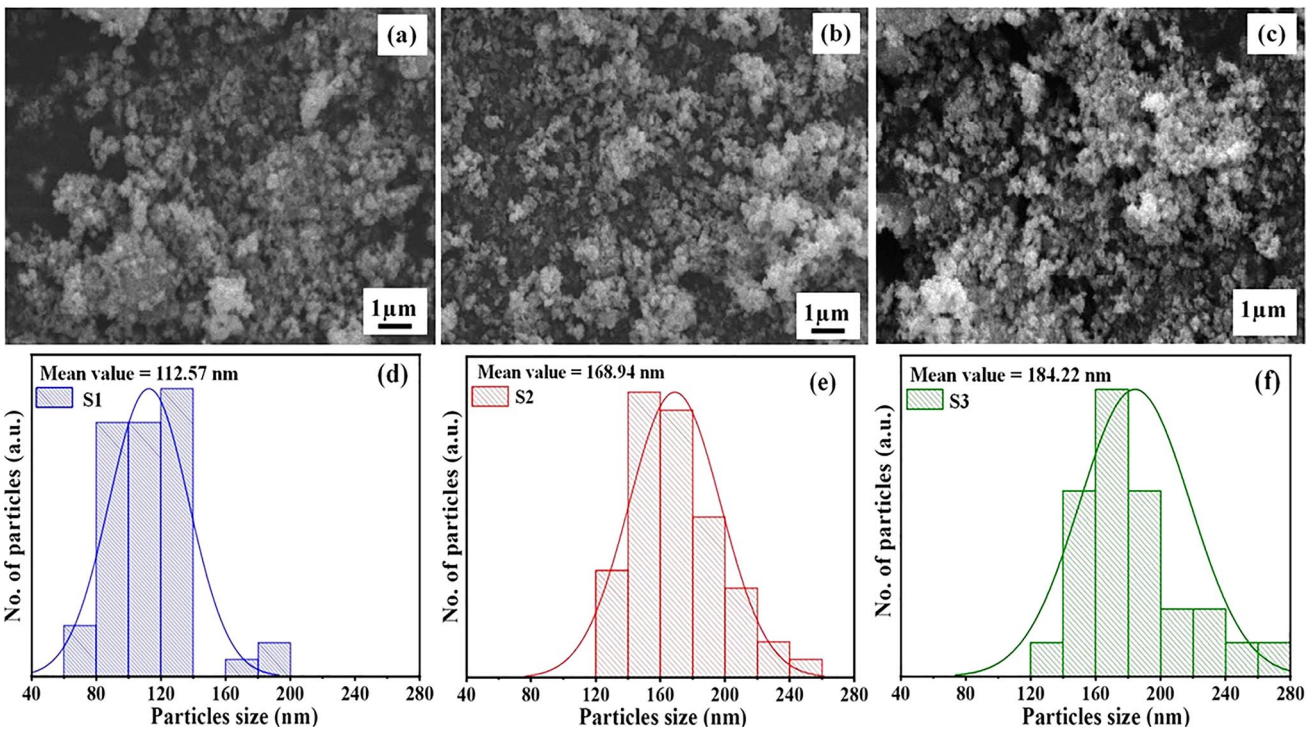

Fig. 3 SEM images of CuS nanoparticles synthesized utilizing leaf extracts of (a) neem (S1), (b) jamun (S2), and (c) kaner (S3) at 1 µm scale. The histogram data for each sample representing the average particle size of nanoparticles for (d) neem (S1), (e) jamun (S2), and (f) kaner (S3).

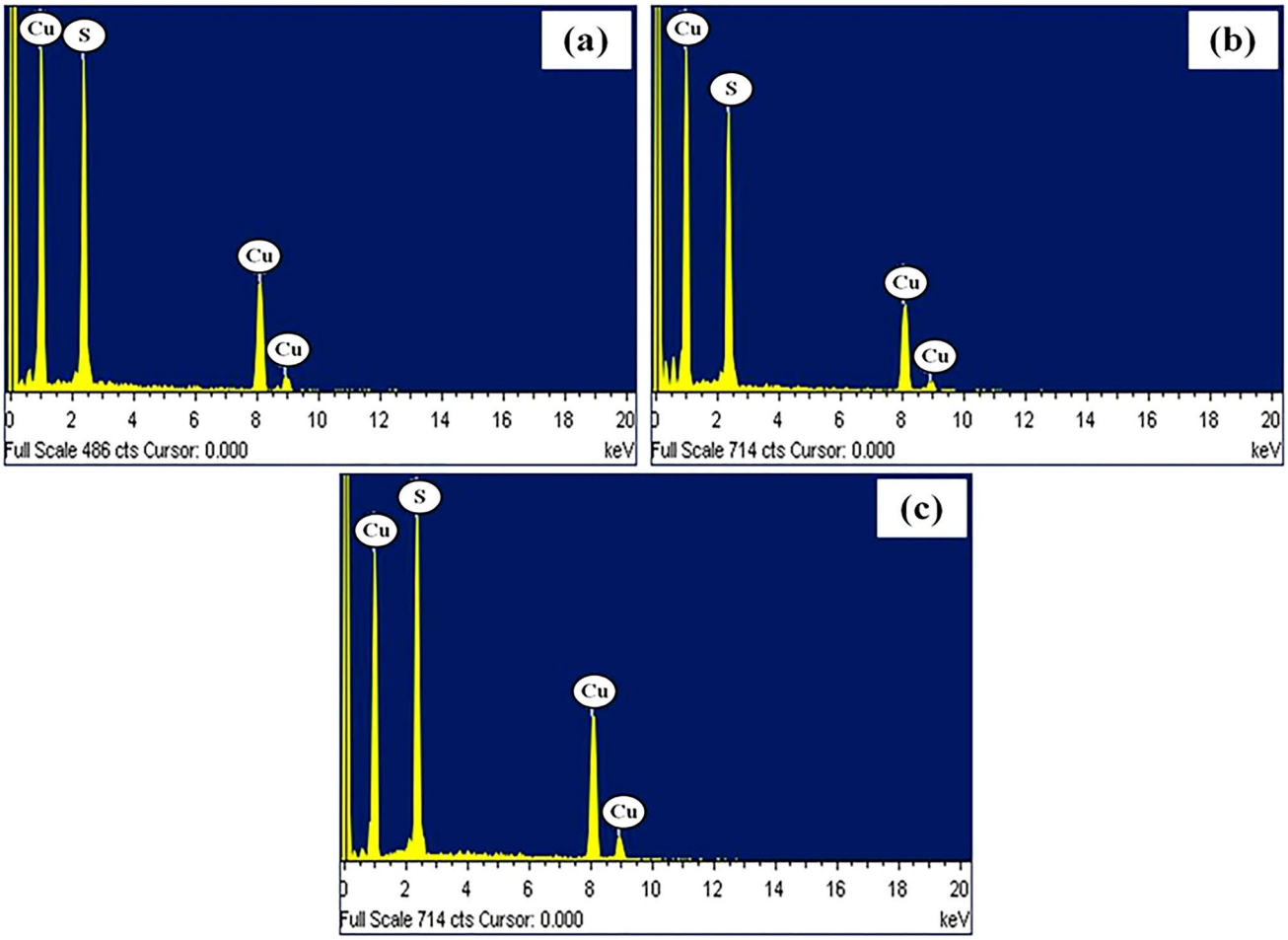

Fig. 4 EDX spectral analysis of CuS nanoparticles: (a) neem (S1), (b) jamun (S2), and (c) kaner (S3).

Table III Elemental identification and their atomic % in all CuS samples

Elemental composition	Atomic %		
	S1	S2	S3
Cu	48.05	47.08	48.00
S	51.95	52.92	52.00

required stoichiometric ratio of Cu and S than the other two samples, and the results are presented in Table III.

Optical Characteristics

Ultraviolet–Visible Spectral Analysis

UV–Vis spectroscopy was used to study the optical behaviour of the green-synthesized samples. The optical absorption for each CuS sample is recorded by analysing the light absorbance peaks at wavelengths ranging from 300 nm to 900 nm as shown in Fig. 5. The optical absorbance edges of

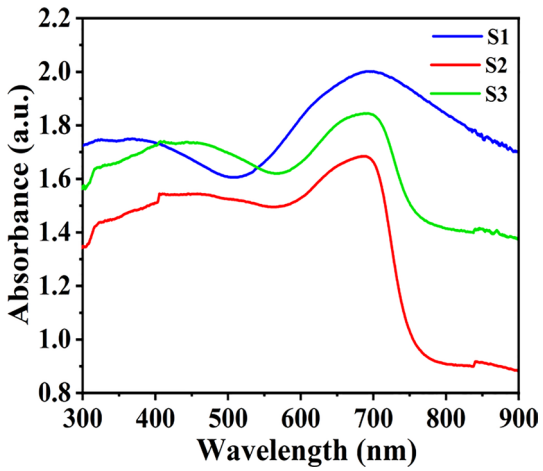

Fig. 5 UV-Vis absorbance spectra of the green-synthesized CuS.

major intensities for S1, S2, and S3 are centered at 694 nm, 687, and 690 nm, respectively, which lie in the red region of visible range of absorbance spectra. The absorption spectra

of each sample show another absorption peak with a wide band of absorption lying within the wavelength range of 300–500 nm. This band may appear as a result of some surface defects present in the samples and may introduce excitonic electronic transitions as inter-band gap states between the occupied valance band and the unoccupied conduction band of CuS.[20]

The recorded wavelength values of optical absorptions for each sample are used to estimate the band gap energies (E_g) for S1, S2, and S3 by applying the Tauc equation (Eq. 8).[45]

$$\alpha h\upsilon = C(h\upsilon - E_g)^n \tag{8}$$

where α represents the absorption coefficient, C is an energy-dependent constant, E_g is the optical band gap, h is the Planck constant, υ is photonic frequency, $h\upsilon$ denotes photon energy, and parameter n is a constant with a value of $1/2$ for the direct band gap. Figure 6a–c depicts the values for the direct energy band gap that are determined by graphs plotted between $(\alpha h\upsilon)^2$ and $(h\upsilon)$ by applying the baseline approach.[46] The calculated values of band gap energies for S1, S2, and S3 are 1.7 eV, 1.6 eV, and 1.5 eV, respectively. S1 displays a comparatively higher optical absorbance in the visible region and a relatively larger energy band gap value than S2 and S3. The reduced energy band gap for S2 and S3 as compared to that of S1 is attributed to the larger particles size of these samples.[47]

Photoluminescence Spectral Analysis

Photoluminescence (PL) spectroscopy probes the optical properties of a material by exciting it with photons of suitable energy. The photoexcited electrons move to a higher excited state and then relax to a lower equilibrium energy state by emitting energy in the form of luminescence. This analysis allows us to understand the electronic transitions, recombination, and separation of photoinduced electron and hole pairs. The PL spectra of S1, S2, and S3 were recorded when they were exposed to an excitation wavelength of 300 nm using the xenon lamp.[21]

Figure 7 shows a relative analysis of excitonic emission spectra of respective samples plotted between PL intensity and wavelength. The emission peaks for CuS samples are detected within the wavelength range of 300–600 nm. The notable, stable, and broad emission peaks for S1, S2, and S3 are observed at 387 nm which confirms their excitonic emissions in the visible region. The monotonic lowering of emission intensities indicates the decreased recombination

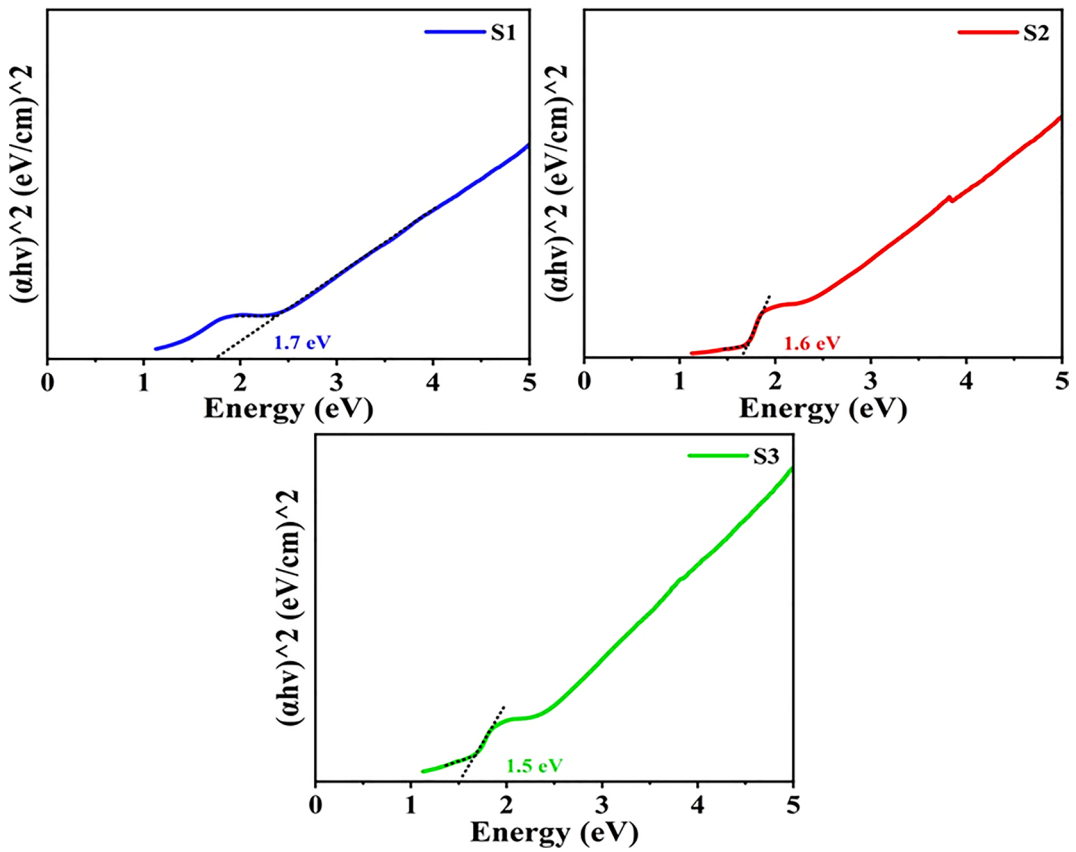

Fig. 6 Tauc's plot for all three green-synthesized samples (a) neem (S1), (b) jamun (S2), and (c) kaner (S3).

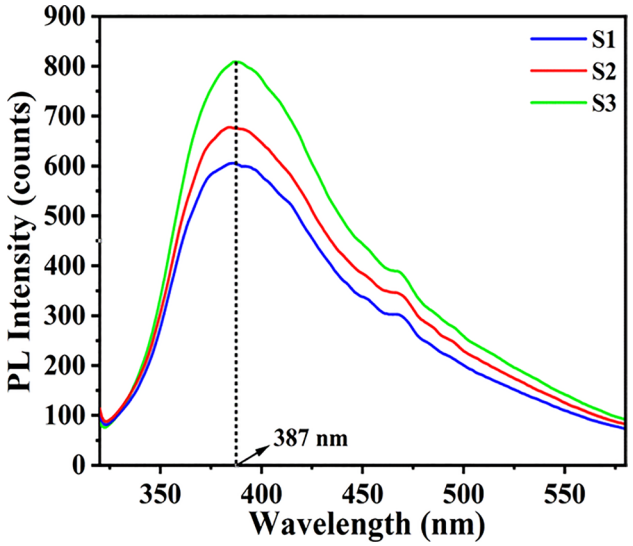

Fig. 7 PL (emission) spectra of the green-derived samples.

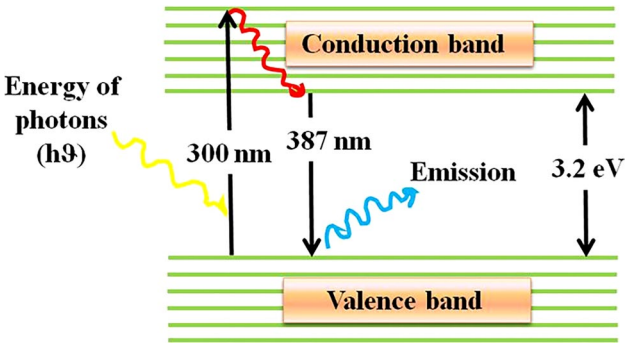

Fig. 8 A plausible representation of the luminescence process for the direct energy band gap of CuS nanoparticles using an energy level diagram.

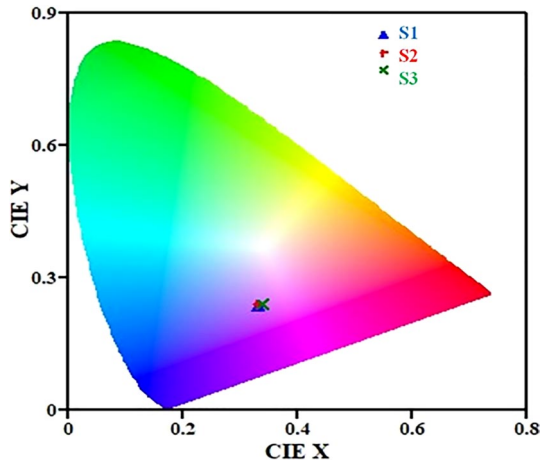

Fig. 9 The CIE 1931 chromaticity diagram for CuS nanoparticles.

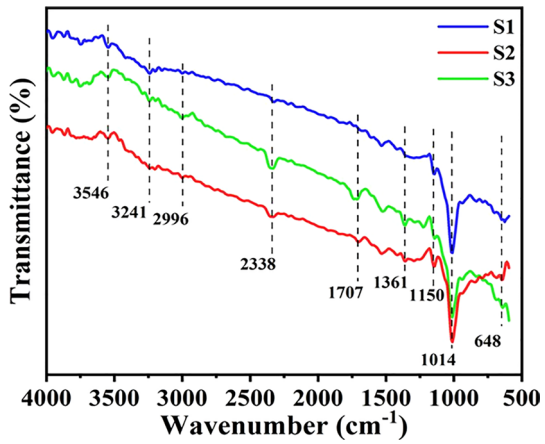

Fig. 10 FTIR spectra of neem (S1), jamun (S2), and kaner (S3) prepared via leaf extracts.

rate of electron–hole pairs. The S1 sample exhibits the lowest recombination rate of charge carriers among the three samples as the emission peak for S1 has the lowest intensity. The possible electronic transitions between the highest occupied molecular orbital (HOMO) of equilibrium state and the lowest unoccupied orbital (LUMO) of excited state are represented by an energy level diagram in Fig. 8, which displays the direct band gap transitions of photoexcited electrons on the excitation of the green-synthesized samples with a wavelength of 300 nm. Notable band edge emission for all three samples as estimated from absorbance spectra was ~350 nm. This value validates the emission wavelength in PL spectra centered at 387 nm with the band gap value of 3.2 eV.

The CIE 1931 colour space is a chromatic representation of CuS nanoparticles as depicted in Fig. 9. The chromatic coordinates for S1 are $(x, y) = (0.33, 0.23)$. For S2, the calculated coordinates are (0.34, 0.23). The colour coordinates for S3 are computed as (0.34, 0.24). The coordinates (x, y) for each sample fall in the blue-violet region of the spectrum, which is close to the white region. This shows that they have potential applications in the fabrication of light-emitting diodes (LEDs).

Vibrational Studies

FTIR Spectral Analysis

The surface chemical composition of the green-synthesized CuS samples was investigated by FTIR spectroscopy over a scan range of 4000–500 cm^{-1} as shown in Fig. 10. The spectra of samples confirm the presence of CuS by detecting a band at 648 cm^{-1} corresponding to Cu–S vibrational stretching mode.[20] A broad band at 3546 cm^{-1} indicates the O–H stretching mode of vibrations which could be the result

of flavonoids present in the synthesized CuS samples.[48] A broad band is observed at 3241 cm^{-1} corresponding to O–H stretching of water molecules. An additional weak and broad band was present at 2996 cm^{-1}, attributed to intermolecular O–H stretching. A weak band that occurred at 2338 cm^{-1} could be the result of absorption of environmental CO_2. A sharp and strong band was obtained at 1014 cm^{-1}, attributed to the C–F stretching mode, which could be from fluoro components of leaf extracts. Other weak and medium bands were detected at 1707 cm^{-1}, 1361 cm^{-1}, and 1150 cm^{-1} corresponding to C–H bending (aromatic compound), O–H bending (phenolic group), and C–N stretching, respectively, in the synthesized samples. The medium band observed at 1150 cm^{-1} corresponding to O–H bending mode confirms the presence of gallic acid in jamun and kaner leaf extracts.[6]

Conclusion

The green synthesis of CuS nanoparticles was successfully carried out by a hydrothermal route employing leaf extracts of neem, jamun, and kaner as solvents. The distinct XRD patterns of the green-synthesized samples match well with ICDD card no. 06-0464, confirming the covellite hexagonal phase of CuS nanoparticles. The XRD analysis indicates the formation of CuS nanoparticles with no impurity peaks. The morphological and elemental analyses confirm the formation of spherical-shaped nanoparticles with slight agglomeration and with only Cu and S. The optical analysis of the neem leaf-based CuS sample (S1), jamun leaf-based CuS sample (S2), and kaner leaf-based sample (S3) shows a consistent decrease in the band gap energies of CuS. S1 exhibits a relatively higher absorbance in the visible region, with a band gap value of 1.7 eV. The CIE plot of the synthesized samples can be used to fabricate LEDs in the blue region. The S1 sample, synthesized with neem leaf extracts, exhibited relatively better structural, morphological, and optical properties and was also shown to be a promising candidate for optical applications.

Acknowledgments Author KM Srishti Barnwal is grateful to the Director of the National Institute of Technology, Kurukshetra, for providing the fellowship. The author also appreciates the support from Dr. Ashish Gupta, Department of Physics, NIT Kurukshetra. The author is grateful to Dr. Sanjeev Aggarwal, Director Ion Beam Centre, Kurukshetra University, Kurukshetra, for providing the XRD facility. The author also acknowledges the Department of Chemistry, Kurukshetra University, Kurukshetra, for providing the FTIR facility.

Author Contributions KM Srishti Barnwal: conceptualization, methodology, investigation, formal analysis, writing—original draft. Yukti Gupta: conceptualization, methodology, investigation, formal analysis, writing—review and editing. Neena Jaggi: supervision, validation, writing—review and editing. KM Srishti Barnwal and Yukti Gupta have contributed equally to this work.

Conflict of interest The authors declare that they have no known competing financial or scientific interests or personal relationships that could have appeared to influence the work reported in this paper.

References

1. S. Deb and P.K. Kalita, Green synthesis of copper sulfide (CuS) nanostructures for heterojunction diode applications. *J. Mater. Sci. Mater. Electron.* 32, 24125 (2021).
2. S. Faisal et al., Green synthesis of zinc oxide (ZnO) Nanoparticles using aqueous fruit extracts of *Myristica fragrans*: their characterizations and biological and environmental applications. *ACS Omega* 6, 9709 (2021).
3. Y. Xie, G. Bertoni, A. Riedinger, A. Sathya, M. Prato, S. Marras, R. Tu, T. Pellegrino, and L. Manna, Nanoscale transformations in covellite (CuS) nanocrystals in the presence of divalent metal cations in a mild reducing environment. *Chem. Mater.* 27, 7531 (2015).
4. A. Morales-García, A.L. Soares, E.C. Dos Santos, H.A. De Abreu, and H.A. Duarte, First-principles calculations and electron density topological analysis of covellite (CuS). *J. Phys. Chem. A* 118, 5823 (2014).
5. J. Kundu and D. Pradhan, Influence of precursor concentration, surfactant and temperature on the hydrothermal synthesis of CuS: structural, thermal and optical properties. *New J. Chem.* 37, 1470 (2013).
6. D. Borah, P. Saikia, P. Sarmah, D. Gogoi, J. Rout, N.N. Ghosh, and C.R. Bhattacharjee, Composition controllable alga-mediated green synthesis of covellite CuS nanostructure: an efficient photocatalyst for degradation of toxic dye. *Inorg. Chem. Commun.* 142, 109608 (2022).
7. A.A. Rokade, Y.E. Jin, and S.S. Park, Facile synthesis of plate-like CuS nanoparticles and their optical and photo-thermal properties. *Mater. Chem. Phys.* 207, 465 (2018).
8. B. Pejjai, M. Reddivari, and T.R.R. Kotte, Phase controllable synthesis of CuS nanoparticles by chemical co-precipitation method: effect of copper precursors on the properties of CuS. *Mater. Chem. Phys.* 239, 122030 (2020).
9. I. Savarimuthu and M.J.A.M. Susairaj, CuS nanoparticles trigger sulfite for fast degradation of organic dyes under dark conditions. *ACS Omega* 7, 4140 (2022).
10. M. Huston, M. Debella, M. Dibella, and A. Gupta, Green synthesis of nanomaterials. *Nanomaterials* 11, 2130 (2021).
11. M. Li et al., Effect of the annealing atmosphere on crystal phase and thermoelectric properties of copper sulfide. *ACS Nano* 15, 4967 (2021).
12. Y. Liu, M. Ji, and P. Wang, Recent advances in small copper sulfide nanoparticles for molecular imaging and tumor therapy. *Mol. Pharm.* 16, 3322 (2019).
13. S. Goel, F. Chen, and W. Cai, Synthesis and biomedical applications of copper sulfide nanoparticles: from sensors to theranostics. *Small* 10, 631–645 (2014).
14. M. Saranya and A.N. Grace, Hydrothermal synthesis of CuS nanostructures with different morphology. *J. Nano Res.* 18–19, 43 (2012).
15. B. Pejjai, M. Reddivari, and T.R.R. Kotte, Phase controllable synthesis of CuS nanoparticles by chemical co-precipitation method: effect of copper precursors on the properties of CuS. *Mater. Chem. Phys.* 239, 122030 (2020).
16. C. Nethravathi, R. Nath, J.T. Rajamathi, and M. Rajamathi, Microwave-assisted synthesis of porous aggregates of CuS nanoparticles for sunlight photocatalysis. *ACS Omega* 4, 4825 (2019).

17. M. Khademian, M. Zandi, M. Amirhoseiny, and D. Dorranian, Synthesis of CuS nanoparticles by laser ablation method in DMSO media. *J. Clust. Sci.* 28, 2753 (2017).
18. S. Riyaz, A. Parveen, and A. Azam, Microstructural and optical properties of CuS nanoparticles prepared by Sol-Gel route. *Perspect. Sci.* 8, 632 (2016).
19. M. Pal, N.R. Mathews, E. Sanchez-Mora, U. Pal, F. Paraguay-Delgado, and X. Mathew, Synthesis of CuS nanoparticles by a wet chemical route and their photocatalytic activity. *J. Nanoparticle Res.* 17, 1 (2015).
20. Y. Gupta and N. Jaggi, Integrated hydrothermal-green synthesis approach for covellite CuS nanoparticles with enhanced energy bandgap for BLEDs. *J. Mater. Sci. Mater. Electron.* 34, 2014 (2023).
21. R.R. Nayak, T. Gupta, and R.P. Chauhan, Plant metabolites assisted green synthesis of ZnSe: structural, optical and transport properties. *Chem. Pap.* 76, 6607 (2022).
22. V.V. Makarov, A.J. Love, O.V. Sinitsyna, S.S. Makarova, and I.V. Yaminsky, Green nanotechnologies: synthesis of metal nanoparticles using plants. *Acta Naturae* 6, 35 (2014).
23. O. Długosz, J. Chwastowski, and M. Banach, hawthorn berries extract for the green synthesis of copper and silver nanoparticles. *Chem. Pap.* 74, 239 (2020).
24. S. Slathia, T. Gupta, and R.P. Chauhan, Green synthesis of Ag–ZnO nanocomposite using *Azadirachta indica* leaf extract exhibiting excellent optical and electrical properties. *Phys. B Condens. Matter* 621, 413287 (2021).
25. C. R. Lett, UV-visible absorption spectra of synthesized CDS nanoparticles and tau plot is shown in Figure 3 (a & b). The calculated energy band-gap of synthesized CdS-NP s Was 3. 31 EV which is higher as compared to bulk CdS (2.42 EV) due to the presence of Q, **4**, 98 (2021).
26. P. Rawat, A. Nigam, and S. Kala, Green synthesis of copper and copper sulfide nanoparticles. *AIP Conf. Proc.* 2220, 020102 (2020).
27. B. Bonigala, A.A. Manne, Y. Saraswathi, U.K. Mangamuri, P.B. Bondili, and S. Poda, Ecofriendly synthesis physicochemical characterization and catalytic activity of gold nanoparticles using plants. *Int. J. Adv. Scientific Res. Manag* 3, 124 (2018).
28. T. Riaz et al., Phyto-mediated synthesis of nickel oxide (NiO) Nanoparticles using leaves' extract of *Syzygium cumini* for antioxidant and dyes removal studies from wastewater. *Inorg. Chem. Commun.* 142, 109656 (2022).
29. J.F. Islas, E. Acosta, Z.G. Buentello, J.L. Delgado-Gallegos, M.G. Moreno-Treviño, B. Escalante, and J.E. Moreno-Cuevas, An overview of neem (Azadirachta Indica) and its potential impact on health. *J. Funct. Foods* 74, 104171 (2020).
30. M. Ahmed, D.A. Marrez, N. Mohamed Abdelmoeen, E. Abdelmoneem Mahmoud, M.A.S. Ali, K. Decsi, and Z. Tóth, Studying the antioxidant and the antimicrobial activities of leaf successive extracts compared to the green-chemically synthesized silver nanoparticles and the crude aqueous extract from *Azadirachta indica*. *Processes* 11, 1644 (2023).
31. M. Arumugam, D.B. Manikandan, E. Dhandapani, A. Sridhar, K. Balakrishnan, M. Markandan, and T. Ramasamy, Green synthesis of zinc oxide nanoparticles (ZnO NPs) using *Syzygium cumini*: Potential multifaceted applications on antioxidants, cytotoxic and as nanonutrient for the growth of *Sesamum indicum*. *Environ. Technol. Innov.* 23, 101653 (2021).
32. A.N. Khan, N.N. Ali Aldowairy, H.S. Saad Alorfi, M. Aslam, W.A.B. Bawazir, A. Hameed, and M.T. Soomro, Excellent antimicrobial, antioxidant, and catalytic activities of medicinal plant aqueous leaf extract derived silver nanoparticles. *Processes* 10, 1949 (2022).
33. B. Poojar et al., Methodology used in the study. *Asian J. Pharm. Clin. Res.* 7, 1 (2017).
34. I.S. Che Sulaiman, M. Basri, H.R. Fard Masoumi, W.J. Chee, S.E. Ashari, and M. Ismail, Effects of temperature, time, and solvent ratio on the extraction of phenolic compounds and the anti-radical activity of *Clinacanthus nutans* lindau leaves by response surface methodology. *Chem. Cent. J.* 11, 1 (2017).
35. I.E. Aouissi, S. Chandren, N. Basar, and W.N. Wan Ibrahim, Phytochemical-assisted synthesis of titania nanoparticles using *Azadirachta indica* leaf extract as photocatalyst in the photodegradation of methyl orange. *Bull. Chem. React. Eng. Catal.* 17, 683 (2022).
36. R.M. Borges, P.E.R. Bitencourt, C.S. Stein, G.V. Bochi, A. Boligon, R.N. Moresco, and M.B. Moretto, Leaves and seeds of *Syzygium cumini* extracts produce significant attenuation of 2,2 Azobis-2-amidinopropane dihydrochloride-induced toxicity via modulation of ectoenzymes and antioxidant activities. *J. Appl. Pharm. Sci.* 7, 037 (2017).
37. J. Ramaraj, S. Ramya, K. Neethirajan, and R. Jayakumararaj, profile of bioactive compounds in *Syzygium cumini*-a review. *Artic. J. Pharm. Res.* 5, 4548 (2013).
38. X. Liu, J. Wang, Y. Wang, C. Huang, Z. Wang, and L. Liu, In situ functionalization of silver nanoparticles by Gallic acid as a colorimetric sensor for simple sensitive determination of melamine in milk. *ACS Omega* 6, 23630 (2021).
39. C.F. Holder and R.E. Schaak, Tutorial on powder x-Ray diffraction for characterizing nanoscale materials. *ACS Nano* 13, 7359–7365 (2019).
40. A. Mahana, O.I. Guliy, S.C. Momin, R. Lalmuanzeli, and S.K. Mehta, Sunlight-driven photocatalytic degradation of methylene blue using ZnO nanowires prepared through ultrasonication-assisted biological process using aqueous extract of anabaena doliolum. *Opt. Mater. Amst.* 108, 110205 (2020).
41. I.W. Sutapa, A. Wahid Wahab, P. Taba, and N.L. Nafie, Dislocation, crystallite size distribution and lattice strain of magnesium oxide nanoparticles. *J. Phys. Conf. Ser.* 979, 012021 (2018).
42. J. Li and L.W. Wang, Band-structure-corrected local density approximation study of semiconductor quantum dots and wires. *Phys. Rev. B Condens. Matter Mater. Phys.* (2005). https://doi.org/10.1103/PhysRevB.72.125325.
43. X. Wang, L. Sø, R. Su, S. Wendt, P. Hald, A. Mamakhel, C. Yang, Y. Huang, B.B. Iversen, and F. Besenbacher, The influence of crystallite size and crystallinity of anatase nanoparticles on the photo-degradation of phenol. *J. Catal.* 310, 100 (2014).
44. F. Pellegrino, L. Pellutiè, F. Sordello, C. Minero, E. Ortel, V.-D. Hodoroaba, and V. Maurino, Influence of agglomeration and aggregation on the photocatalytic activity of TiO_2 nanoparticles. *Appl. Catal. B Environ.* 216, 80 (2017).
45. J. Tauc, *STATES I N T H E GAP* 10, 569 (1972).
46. T. Tauc, P. Kubelka, F. Munk, S. Information, and T. Tauc, How to correctly determine the band gap energy of modified semiconductor photocatalysts based on UV—Vis spectra, 8 (2018).
47. M. Singh, M. Goyal, and K. Devlal, Size and shape effects on the band gap of semiconductor compound nanomaterials. *J. Taibah Univ. Sci.* 12, 470 (2018).
48. X. Liu, *Organic chemistry I* (Surrey: Kwantlen Polytechnic University, 2021).